SAND2017-4512J

LASER-DIAGNOSTIC MAPPING OF TEMPERATURE AND SOOT STATISTICS IN A 2-m DIAMETER TURBULENT POOL FIRE

Sean P. Kearney and Thomas W. Grasser

Engineering Sciences Center
Sandia National Laboratories
Albuquerque, NM 87185 USA

Submitted to Combustion and Flame

Abstract

We present spatial profiles of temperature and soot-volume-fraction statistics from a sooting 2-m base diameter turbulent pool fire, burning a 10%-toluene / 90%-methanol fuel mixture. Dual-pump coherent anti-Stokes Raman scattering and laser-induced incandescence are utilized to obtain radial profiles of temperature and soot probability density functions (pdf) as well as estimates of temperature/soot joint statistics at three vertical heights above the surface of the methanol/toluene fuel pool. Results are presented both in the fuel vapor-dome region at ¼ base diameter and in the actively burning region at ½ and ¾ diameters above the fuel surface. The spatial evolution of the soot and temperature pdfs is discussed and profiles of the temperature and soot mean and rms statistics are provided. Joint temperature/soot statistics are presented as spatially resolved conditional averages across the fire plume, and in terms of a joint pdf obtained by including measurements from multiple spatial locations.

Keywords: Fire research; pool fire; soot; laser diagnostics

1. Introduction

Fire is a leading threat to the security of transportation systems and critical infrastructure, and is a critical factor in life-safety considerations. Improved computational tools for risk assessment increasingly rely upon solid physical underpinnings for predictive simulation of fire phenomena. Fire fluid-dynamics codes must capture complex, multi-physics effects, encompassing turbulent mixing, chemical reaction, and the thermal radiative transport that is a product of the reacting flow—all in a three-dimensional system that is several meters or more in size. To achieve realistic, fully turbulent condtions, buoyancy-dominated fire plumes must be at least 1 meter in base size [1, 2]. At this length scale, simulations are costly, so that detailed experiments are extraordinarily valuable for development of subgrid and engineering models that make calculations more tractable, and for validation of fire simulations.

Radiative heat transfer from hot soot is the primary threat from a fire-accident scenario. In the absence of scattering, the radiative transfer equation along a linear path, s, through the fire plume is given by

$$\frac{\overline{dI_\lambda(s)}}{ds} = \overline{\mu_\lambda(s) I_{\lambda,b}(s;T)} - \overline{\mu_\lambda(s)}\;\overline{I_\lambda(s)} \quad , \tag{1}$$

where the overbars represent time averaging, I_λ is the radiative intensity along s; $I_{\lambda,b}$ is the blackbody spectral intensity at the local temperature, T; and μ_λ is the absorption coefficient. The soot-volume-fraction, f_v, dependence of μ_λ is $\mu_\lambda = g(n) f_v/\lambda$, where g is a function of the soot refractive index, n, and λ is the wavelength [3]. Experimental validation of Eq. 1 then requires measurement of the local temperature and soot volume fraction along a path through the fire plume, and this expression simply states that the change in radiation intensity along s is emission minus absorption. In the absorption term, μ_λ and I_λ may be treated with independent time-averaging operations because correlation is weak

between the radiative intensity, which is influenced by long-range contributions, and μ_λ, which is entirely determined by the structure of the local soot field. Soot radiative emission, represented by the first term on the right-hand side of Eq. 1, originates from thin soot layers [4-8], where high gradients in both temperature, and soot concentration may exist. Correlation between these two locally determined quantities can be quite significant and the $\mu_\lambda I_{\lambda,b}$ product must be averaged as a single quantity, necessitating simultaneous space- and time-coincident temperature/soot measurements. Ideally, sufficient sampling should be acquired to obtain estimates of the joint pdf of the temperature and soot fluctuations, which can then be utilized to develop emission source terms for fire heat-flux calculations in turbulent flames and fire plumes.

Simultaneous space- and time-resolved measurement of temperature and soot in a turbulent combustion environment represents a significant measurement challenge, but some examples can be found in the literature. Emission probes provide a direct measurement of soot temperature integrated over a volume and can be coupled with laser light extinction to yield soot f_v. Sivathanu and Faeth [9] report simultaneous T/f_v data from laboratory-scale, buoyant, turbulent diffusion flames using two-color pyrometry and laser light extinction. The measurements were path integrated over a 1- to 2-cm extent, with a corresponding volumetric spatial resolution of 0.067–0.135 cm^3. They presented temperature probability densities (pdf) conditioned on soot f_v, which revealed that soot exists in a relatively narrow range of temperatures within the underfire (fuel-rich) region and additionally analyzed scalar state relationships data from earlier work [10, 11] in the overfire (fuel-lean) region to infer a much wider range of soot temperatures there. More recently, Mahmoud and co-workers [6] performed highly spatially resolved, two-dimensional T/f_v imaging in a sooting turbulent jet flame, using laser-induced fluorescence of indium and soot laser-induced incandescence (LII). These data were used to estimate soot pdfs conditioned on temperature. Their conclusions regarding soot temperature history were

consistent with Sivathanu and Faeth's [9]; soot experiences a narrow range of temperatures low in the flame and early in its history, and then proceeds to occupy a larger range of temperatures with residence time as it is transported upward and experiences a variety of conditions relative to the reaction zone. Mahmoud *et al.* [6] examined their joint T/f_v pdf data to conclude that soot temperature displayed little radial dependence, and that the horizontal structure of the mean soot profile was due solely to the increase in intermittency of soot fluctuations with radial distance. Mahmoud *et al.* observed log-normal conditional soot pdfs across the full range of temperatures, which is associated with a high degree of intermittency in soot turbulent fluctuations. Soot intermittency is a well-known phenomenon, and has been observed in LII measurements in jet flames [5, 12, 13], buoyancy dominated flames at lab scale [4, 7], and meter-scale pool fires of moderate sooting propensity fuels [8].

We located two studies devoted to simultaenoues T/f_v measurements in fully turbulent, meter-scale pool fires. Gritzo *et al.* [14] deployed a water-cooled optical probe in a 6-m JP-8 pool fire and report pyrometer temperatures and emission/absorption soot volume fractions within a 2-cm-long × 1-cm-diameter sampling volume. Their results revealed a conditionally averaged soot temperature that was essentially invariant to soot concentration at a single location near the center of the fire plume. Murphy and Shaddix [15] used a similar fiber-optically coupled diode-laser probe to Gritzo *et al.* for extinction/absorption measurements of soot volume fraction, along with two-color pyrometry in a 1-m-diameter, turbulent JP-8 pool fire. The measurement path length was 3.6 cm and the collection aperture was 5.5 mm. Soot pdf data conditioned on emission temperature displayed a departure from the log-normal form observed by others in turbulent jet flames [5, 7] and pool fires of more lightly sooting liquid fuel blends [8], representing significant reduction in the intermittency of soot fluctuations near the center of these heavily sooting fire plumes.

These earlier pool-fire measurements, while revealing, were still limited in their volumetric spatial resolution (0.8–1.5 cm^3), and subject to the usual assumptions associated with two-color pyrometry. We have more recently described laser-diagnostic instrumentation for temperature and soot measurements in meter-scale fire plumes at volumetric spatial resolutions as fine as 10^{-4} cm^3 for temperature and 10^{-5} cm^3 for soot by utilizing dual-pump coherent anti-Stokes Raman scattering (CARS) thermometry [16, 17] and LII [18]. This work was facilitated by the Sandia Fire Laboratory for Accreditation of Models and Experiments (FLAME) facility [19], which allows for controlled meter-scale burns with integrated laser diagnostics. Our earlier work demonstrated capability, but provided limited data at only a single measurement location, and for a restricted number of laser shots and fire realizations that was too small for meaningful statistics to be generated. In this article, we will present the application of these laser-diagnostic tools in a more significant data campaign, where temperature/soot statistics were mapped across the radial extent of a 2-m base diameter fire plume at three vertical heights above the fuel surface. Large ensembles consisting of tens of thousands of single-laser-shot measurements, obtained over multiple fire experiments, are used to gather more meaningful statistical results. We present the data here in terms of radial profiles of temperature and soot statistical quantities and provide joint statistical estimates in the form of both mean soot and soot pdf, both conditioned on CARS temperature data.

2. FLAME Facility

The design and construction of FLAME (Fire Laboratory for Accreditation of Models and Experiments) is shown in Figure 1 and described in significant detail by Blanchat *et al*. [19] and by Kearney *et al.* [16]. Briefly, a 2-m fuel pan is located at the center of an 18.3-m diameter × 12.2-m high main test bay level, whose water-cooled walls provide a well-controlled ambient temperature far-field condition. Combustion air is provided through a well-balanced air ring at the periphery of the FLAME

basement level and entrained through steel-grated flooring at the perimeter of the main test-bay level. A smooth ground plane is provided by a 12-m outer-diameter steel skirt that surrounds the fuel pan. Constant liquid fuel level is maintained just below the pan tip throughout the experiment by supplying fuel at a rate adjusted by real-time monitoring of the surface liquid level. A research fuel blend of 10% toluene by volume in a balance of methanol is used in our experiments. The flame height of the resulting 2-m base diameter fire plume is ~2.5 m based on time-exposed imaging of visible soot emission, with a time-dependent structure that is dominated by periodic "puffing" motion characteristic of large, buoyancy driven fires [20]. Addition of heavily sooting toluene to clean-burning methanol allows us to achieve a balance between fuel sooting propensity, fire optical thickness, and heat transfer to optical elements located in proximity to the fire plume; thereby facilitating application of laser diagnostics, but representing a compromise as soot yield is lower than if a real transportation fuel were to be burned. The resulting pool fire, shown in Figure 2, has much of the turbulence properties as a jet-fuel burn, albeit with reduced soot levels. The observed soot fluctuations to be reported here were typically on the order of 100s of parts per billion (ppb), with a high level of intermittency that results in mean volume fractions of just a few ppb. This contrasts a transportation-fuel fire, which would exhibit soot layers with a few parts per million (ppm) of soot.

A photograph of the FLAME test-bay level with the fuel pan, optical hardware enclosures, and vertical positioning platforms is shown in Figure 3. Three water-cooled enclosures housed the CARS beam-crossing lens, LII focusing lens, CARS collection optics [16, 17], and the LII imaging optics [8] adjacent to the fire plume. These enclosures are mounted to three individually adjustable precision lifting platforms, which can position the measurement volume anywhere from 0.5 to 1.8 m above the fuel-pool surface in conjunction with a remotely controlled laser-beam periscope, which is not shown in the Figure. The fuel pan is mounted to a rail system for horizontal translation over a 1-m range of travel

using a remotely actuated motor. All drive motors, pulleys and control systems are located at the FLAME basement level to shield this equipment from heat and flames. Thermal expansion of lifting platform supports exposed to fire radiative fluxes is minimized with judicious choice of materials and by insulating the supports with 50-mm thick "kaowool" jackets wrapped in a reflecting stainless-steel foil. This arrangement allows us to maintain sufficient CARS signal for up to an hour or more of burn time, over which the fuel pan is horizontally scanned with the optics maintained at constant height. CARS and LII data are obtained on a single-laser-shot basis, with several thousand laser shots acquired at each radial location before moving the fuel pan. Data are first acquired in the hottest regions, near the center of the fire, so that degradation of the CARS signal strength due to thermally induced optical misalignment and fouling of optics over the course of an experiment is balanced by increased CARS signals in the colder gas that is encountered as the measurement volume is scanned radially outward. Laser-diagnostic data have been acquired at heights of 0.5, 1.0 and 1.5 m above the 2-m diameter fuel pool. Multiple burns were conducted at each measurement height to both increase the size of the data ensemble and to capture any effects of day-to-day variation of the FLAME test bay conditions. During the course of a single burn, nominally 10,000 to 20,000 laser shots were acquired at points near the center of the fire plume, with a lesser number (2,000 to 10,000) acquired at outer locations where less soot and high temperature fluctuations occurred. A total of 5 burns were conducted with the measurement location at y = 1.0 m above the liquid surface, with 3 burns each at y = 0.5 and 1.5 m.

3. Laser-Diagnostic Instrumentation

3.1 CARS Instrument

Design and performance of our dual-pump CARS and LII instruments are described in detail in refs. [16-18], and are summarized here with additional details pertinent to the present study provided. A

schematic of the CARS laser and detection systems is provided in Figure 4. All laser sources are located in a remote laser laboratory, located adjacent to the FLAME test bay. For CARS, an injection-seeded, frequency-doubled Nd:YAG laser pumps a narrowband, frequency-tunable commercial dye laser and a home-built broadband dye source. The two frequency-narrow CARS pump beams at 532 and 554 nm, and the broadband Stokes beam centered at 607 nm are arranged in a folded phase-matching configuration [21] and ported through an AR-coated BK-7 laser window into the FLAME test bay. Typical laser-pulse energies are ε = 50, 50 , and 30 mJ/pulse for the pump-1, pump-2, and Stokes beams, respectively. All laser beams are mirror coupled by a height-adjustable, remote-controlled periscope to a 1000-mm focal length, 50-mm-diameter CARS beam-crossing lens, which is mounted in a water-cooled enclosure adjacent to the pool fire, indicated in Figure 3. CARS signal radiation is generated near 491 nm, in a spectral region where interference from laser-generated C_2 emission [22] and C_2 Raman [23] interferences are minimized. A second water-cooled enclosure, also seen in Figure 3, is located opposite the beam-crossing lens, where an additional 1000-mm focal-length lens collimates the CARS beam, and dichroic mirrors separate the CARS signal from the pump and Stokes radiation. The CARS beam is launched into a 100-μm-core multimode fiber, which transmits the signal for detection by a 0.75-m spectrometer and back-illuminated CCD located in the main laser lab. Each of the steel light pipes seen in Figure 3 taper to a 25-mm diameter at approximately 100 mm from the measurement volume, resulting in a 200-mm beam path through the pool fire gases.

For N_2 CARS, peak signal intensities can vary by a factor of 10^3 between room temperature and flame conditions, which places dynamic range of the CARS detection system at a premium in the highly fluctuating, turbulent fire-plume environment. In order to meet this challenge, we employ a CCD detector with a large well depth of one million e^- in its readout register and divide the image of the dispersed CARS signal beam into as many as 4 vertically-binned segments before detector readout. For

processing, we consider a spectrum as "valid" if its peak spectral intensity is a minimum of 550 e^- above background (peak signal-to-noise ~ 20) and any if one of the vertically-binned segments was below the 16-bit saturation level of the detector's A-D converter. Using these criteria, the best data yield is observed in the measurements at y = 1-m above the fuel pan, where 91% of the acquired CARS spectra were deemed valid. At heights of y = 0.5 m and 1.5 m, valid CARS detection rates were 80% and 84%, respectively.

CARS temperatures are deduced by performing theoretical fits to the N_2 Q-branch portion of the Raman spectrum using the Sandia CARSFT code [24]. Temperature, relative nonresonant-background contribution, and parameters accounting for horizontal and vertical shifts in the spectra are varied in CARSFT. The precision of the single-laser-shot CARS temperatures is estimated at ±3.5-5% with an accuracy of 2-3%, based on measurements in tube-furnace-heated air at 300-1400 K [16]. We retain 90% of the evaluated single-shot spectra and discard 10% of the data that display the poorest fitting residuals. Nitrogen self line broadening is assumed due to lack of knowledge of the shot-to-shot collision partner distribution. Previous work [25] shows that neglect of N_2 Q-branch line broadening by water and CO_2 can result in a 2% overestimation at high temperatures in methane/air combustion. We might expect similar product concentrations for the methanol/toluene fuel, where the neglect of foreign-gas broadening could result in a maximum systematic error of +20–45 K for T = 1000-2200 K, which may add a high-temperature bias to the measurement accuracy observed in the tube-furnace results. As a check, we performed measurements at flame temperatures at T = 1800-2200 K in the product gases of near-adiabatic CH_4/air flames stabilized on the Hencken burner [26], and found the CARS measurements to be within 50 K or less of the expected equilibrium temperatures for flames as rich as ϕ = 1.3.

The volumetric spatial resolution of the CARS measurements is 10^{-4} cm^3, based on a ~100-μm nominal beam focus and a rather long ~8-10 mm beam-overlap region, over which the temperature is not uniform in the fire plume environment. Such a long measurement volume was necessitated by the need to use long (1000 mm) focal length CARS beam-crossing and collimating lenses to locate the CARS optics at the edge of the 2-m fire plume and minimize the amount of time the optical enclosures were engulfed in flames. Fitting of the CARS spectra provides a close approximation to the enthalpy-pooled thermodynamic average temperature[+] within the measurement volume, which is useful because this is the temperature that is most often calculated by computational models. CARS temperatures can be subject to a low-temperature bias due to spatial-averaging or "density-weighting" effects if significant thermal gradients exist along the beam-overlap direction, which forms the major axis of an approximately ellipsoidal CARS measurement volume. Previous studies [27-29] used synthetically generated CARS spectra to provide estimates of spatial averaging errors based on a worst-case scenario of a steep temperature gradient aligned with the measurement-volume axis. They concluded that CARS temperatures track the enthalpy-pooled mean temperature to within 100 K or less if the temperature change $\Delta T = T_{max} - T_{min}$ is less than ~1000 K over the sample volume length.

We have observed the temperature profile along the major axis of the CARS volume for conditions at the radial center of a methanol fire plume at y = 1.0 m above fuel level by using Rayleigh scattering from the CARS pump beams [17]. Clean-burning pure methanol was used as a surrogate fuel for the Rayleigh measurements, which require a flame free of soot. Turbulence properties and gradients in the pure methanol fire are expected to closely approximate those in the sooting 10%-toluene/90%-methanol fuel blend. Single-laser-shot Rayleigh-measured temperature profiles along the axis of the CARS

[+] The enthalpy-pooled temperature is related to the total thermodynamic enthalpy of the gas in the measurement volume through $H = mC_pT$, where m represents the mass of the probed gas, C_p is the specific heat, and T is the enthalpy-pooled average temperature of the combustion gases.

volume are shown in Figure 5a. The two profiles indicated as "typical" on the plot legend are indicative of modest gradients in the measurement volume, with overall temperature excursions, ΔT = xxx and yyy K. The profile indicated as "large gradient" represents the worst-case scenario studied in [27-29]—specifically a flame sheet with a high local temperature gradient along the measurement-volume axis. A histogram of the measured ΔT from 2000 single-laser-shot Rayleigh measurements is shown in Figure 5b. The temperature changes along the axis of the CARS volume is 1000 K or less for 98% of the total Rayleigh measurements, with 90% of the results exhibiting temperature changes less than 600 K. In addition the worst-case scenario of a flame sheet orthogonal to the CARS axis is not observed in the vast majority of laser shots; modest local gradients as shown by the "typical" profiles of Figure 5a are the norm. We calculated synthetic CARS spectra for similar thermal changes within the measurement volume, which indicate that spatial-gradient effects bias best-fit CARS temperatures by only a few 10s of K to perhaps 50 K from the enthalpy-pooled mean on the vast majority of laser shots. Based on these observations, we fell the CARS-average temperature is a good approximation to the thermodynamic-mean value.

3.2 LII Instrument

For LII, a second *Q*-switched Nd:YAG laser provides an 8-ns 1064-nm laser pulse. The LII beam is formed into a nominally 5-mm-high × 1-mm-thick sheet, coincident with the CARS measurement volume, as shown in Figure 6. A combination of cylindrical and spherical lenses located in the remote laser lab, and shown in Figure 7, are used in conjunction with the CARS beam-crossing lens to form the LII laser sheet. The 1064-nm LII laser beam is delivered to the measurement volume through the same steel light pipe used for delivery of the CARS pump and Stokes beams. LII is generated in the plateau-level regime [30, 31] with a beam fluence near 2 J/cm^2, and imaged using a nitrogen-purged, water-

cooled optical assembly described in detail in ref. [18], and also shown in Figure 7. This probe contains heat-rejecting filters and achromatic lenses that relay image the LII laser sheet plane onto the face of a coherent fiber-imaging bundle that transmits the signal to a gated, intensified CCD detector at the FLAME basement level.

Prior to each experiment, the field of view of the LII imaging optics is positioned to be coincident with the CARS measurement volume by observing Rayleigh scattering from the CARS laser beams in air and translating the LII optics so that the beam crossing was centered on the LII camera. The LII images are calibrated for soot volume fraction using the procedure described in [8], which compares LII intensities and 1064-nm laser light-extinction measurements from a Santoro-style C_2H_4/air laminar diffusion flame [32] that is brought into the FLAME test bay. Light-extinction calibration is time consuming and not performed daily, but LII imaging in the Santoro flame was checked each day to monitor any drifts in the LII system response. Peak LII counts from the Santoro reference flame varied by no more than ±20% over the course of the data campaign presented here. We have previously estimated the uncertainty of the single-laser-shot, soot-volume fraction data [8], where systematic error arising from uncertainty in the light-extinction data and soot optical properties are ±23%, and random errors arising from detector shot noise and image intensifier noise are ±34–55% at representative soot loadings of f_v = 0.5 and 0.1 ppm, respectively.

Single-laser-shot LII images are recorded at 10 Hz, with the LII laser pulse arriving 10 μs before the CARS pump and Stokes beams. Recent work by Nordström *et al.* [33] has shown that laser-heated soot from the LII process can transfer heat to the gas-phase on microsecond time scales, with temperature rises as high as 100 K observed at 10 μs delay. We were unaware of this gas-heating effect when performing our pool-fire measurements. However, inspection of selected CARS measurements recorded at the radial center of the fire plume, where soot loading is maximized, indicated that mean temperatures

for 500-laser-shot CARS ensembles taken with and without LII did not differ substantively. We, therefore, believe that heating of the flame gases by the LII pulse did not impact our temperature measurements for the soot levels and laser fluences used in the present work. This may be reasonable given that Nordström *et al.* performed their measurements under a much higher soot volume loading of 4 ppm than was present in our pool-fire experiments, which would maximize the impact of laser-induced heating in their work.

4. Results and Discussion

4.1 Nature of CARS Spectra and LII Image Data

A shot-averaged CARS spectrum recorded with the measurement volume at a height of y = 0.5 m above the fuel surface at the center of the fuel pan (r = 0) is shown in Figure 9a. This averaged spectrum shows contributions from the N_2 Q branch as well as H_2 S-branch rotational lines. The spectrum exhibits significant nonresonant contribution from unburned hydrocarbons, as revealed by the broad, featureless background and modulation dip in the N_2 signature, and significant contributions from laser-generated C_2. At y = 0.5 m, the CARS measurement volume is located within the so-called "vapor dome" [34] of the fire plume, which is an oxygen-deficient interior near the fuel-pool surface, where significant unburned pyrolized hydrocarbons are present. Significant unburned hycrocarbon at this height above the fuel pool was additionally confirmed by infrared emission spectra that revealed significant absorption in the C-H stretch region near 3.3 μm [35]. We highlight this spectrum because measurements in this fuel-rich region are challenging for many laser-diagnostic approaches. Representative single-laser-shot CARS spectra in the N_2-containing region of the spectrum only are shown in Figure 9b-d. Both measured spectra and the corresponding theoretical fits with evaluated temperatures are shown in each of the three spectra. These spectra were recorded during the same burn, and at the same spatial location

as the shot-averaged spectrum in Figure 9a and illustrate our ability to fit the data for reliable temperature measurements in this challenging fuel-rich region of the fire plume. The spectrum in Figure 9b represents a fit to low-N_2-content gases with significant nonresonant background, while the spectra in Figures 9c and 9d illustrate the nature our CARS spectra in hot gases at T = 1876 K and at a much colder temperature T = 960 K.

Representative single-laser-shot LII images recorded at the same spatial location as the CARS spectra in Figure 9 are shown in Figure 10. These images reveal a two-dimensional slice through complex three-dimensional soot structures with a 1-mm averaging depth in the out-of-plane direction. The uppermost image in Figure 10 reveals soot layers viewed along their edges, which appear as thin structures of a few hundred microns in layer thickness. The lower two images in Figure 10 are examples of soot sheets with their elongated directions largely within the plane of the LII laser sheet, which appear as much thicker structures in their two-dimensional projection. In most cases, the soot LII images exhibit large regions where essentially zero soot is present, with sparse soot-containing layers of volume fraction, f_v, of order several hundred ppb to as high as 1-2 ppm on rare occasions. This highly intermittent spatial structure is typical of the LII data recorded throughout the fire plume, and is consistent with highly intermittent turbulent fluctuations of soot observed in laboratory flames [4, 5, 7, 8, 13].

4.2 Temperature and Soot-Volume-Fraction Statistics

Radial profiles of the mean and rms-fluctuation of temperature and soot f_v for all three heights above the burner surface are shown in Figure 11, where smooth curves are faired through the data points as a guide for the eye. Each profile is the result of a compilation measurements obtained from 3-5 burns conducted on different days over a period of approximately 10 weeks. The error bars on the plots

represent the maximum deviation of the single-burn profiles at a given measurement point. The mean temperature profiles all peak at the radial center of the plume near T = 1400 K, revealing that radiative heat loss in this moderately sooting fire plume is not particularly significant. Peak rms fluctuations near 400–450 K are additionally observed at all three heights above the liquid pool surface. The peak in the rms temperature fluctuation moves inward with increasing height, from r = 30 cm at the near-surface location of y = 0.5 m, to r = 20 and 15 cm at y = 1.0 and 1.5 m, respectively. This behavior is consistent with the "neck down" in the mean structure of the fire plume, with collapse of the vapor dome and movement of the peak mixing regions inward with increasing height.

The soot profiles in Figure 11 are markedly different than the temperature profiles. Within the vapor-dome region, the peak mean soot concentration appears off the centerline near r = 15 cm, with the peak fluctuating soot levels occurring at the same location, removed from the location of peak temperature fluctuations at r = 30 cm. In general, mean soot concentrations are extremely low for the 10/90 toluene/methanol research fuel blend, while the rms fluctuations are an order of magnitude higher than the mean—behavior which is consistent with high intermittency in the soot fluctuations. Higher in the fire plume, the peak mean soot concentration moves to the radial centerline and decays with increasing height, from 6.5 ppb at y = 0.5 m to 5 ppb at y = 1.5 m, in contrast to the temperature statistics, which display a nearly constant peak mean temperature at the centerline, and a peak rms fluctuation that is removed from r = 0.

Probability density functions (pdf) of the temperature fluctuations at all locations were generated by binning all the single-shot CARS data into 50-K wide intervals and constructing histograms, with the results plotted in Figure 12. At all three heights, the evolution of the pdf with increasing distance from the plume center is qualitatively similar. At the center of the plume, the highest temperatures are encountered with minimal mixing of low-temperature gases. The pdf shapes are nominally Gaussian

with a weak high-temperature skew at y = 0.5 m, and a stronger low-temperature skew at y = 1.0 and 1.5 m, where width of the fire plume is reduced and the likelihood of low-temperature gases reaching the centerline increases. The temperature pdfs then become nearly uniform at intermediate radial distances, in the peak turbulent mixing zone where rms fluctuations are maximized, at r = 20 cm low in the plume to r = 10 cm at y = 1.5 m. At large radial distances the temperature pdf data begin to exhibit a shape with significant high-temperature skewness at the outer regions of the plume, where strong large-scale puffing motions [36] result in highly intermittent high-temperature fluctuations on top of an increasingly low-temperature baseline.

Probability density functions of the LII-determined soot volume fractions for all measurement locations are presented in Figure 11. The pdfs were constructed by binning the LII signal from each pixel within a 2.35-mm-high × 8.7-mm-wide cropped region at the center of all the images within the ensemble. The bin width was 100 detector counts, corresponding to a soot volume fraction interval of 12.4 ppb, and resulting in 656 bins over the 8.1 ppm dynamic range of the LII instrument. At all heights above the liquid-fuel surface, the soot pdf data at locations closest to r = 0 exhibit a nearly exponential decay across a wide range of soot f_v. The soot pdf structure appears to transition to a form with two distinct slopes on the log-log scale at more outward radial positions. In all cases, the soot pdf displays a lognormal or "zero-clipped" structure that is consistent with a high degree of intermittency, and with the features of the LII image data of Figure 10, with a most likely value near zero and very large, positive fluctuations.

Our fire plume is similar in size to the large JP-8 transportation fuel fires that have previously been studied [14, 15], but the significantly decreased sooting propensity of our research fuel blend relative to JP-8 results in more sparsely distributed soot layers and likely alters the soot pdf, particularly within the interior of the fire. Murphy and Shaddix [15] present emission/absorption soot f_v data from a 1-m-

diameter JP-8 fire. Their soot-volume-fraction pdf data near the center of the fire plume, where the mean soot f_v at the centerline was ~1 ppm, reveal a low level of soot intermittency, and are much closer to a normal or bi-modal distribution in shape. A zero-clipped soot pdf was observed by Murphy and Shaddix [15] at locations removed from the radial centerline of their 1-m JP-8 fire, where soot intermittency would be expected to be higher due to increased mixing of fire gases with the surrounding air. Murphy and Shaddix also observed clipped soot pdf structure high above the fuel surface, where soot oxidation and/or increased mixing of cold, soot-free gas likely diluted the soot stream. In contrast, Henriksen *et al.* [7], performed soot LII measurements in a smaller 15-cm-diameter JP-8 pool fire, with mean soot f_v of 0.1–0.35 ppm on centerline, and observed a similar zero-clipped pdf structure to our measurements throughout this smaller fire plume. Based on these observations, the nature of the soot pdf in a fire plume is dependent on both fire size, and sooting propensity of the fuel. Large, meter-scale fires with heavily sooting transportation fuels will display low intermittency soot fluctuations in their interior and a different soot pdf structure than if a more lightly sooting fuel, or a small, lab-scale pool flame is studied. We must also note that the emission absorption diagnostics used in the meter-scale JP-8 fire experiments in [15] sampled a much larger spatial extent than the LII measurements in the present work and in the small JP-8 pool fire work in [7], which would make the likelihood of encountering soot on a given realization higher and shift the pdf results away from the zero-clipped structure observed in our results. Spatially averaging our LII data in an effort to compare to a coarser resolution emission/absorption probe did not change the nature of the soot pdfs observed in our toluene/methanol fire.

4.3 Joint Statistics of Temperature and Soot

The statistical results presented for temperature and soot independently above are useful for illustrating the nature of the fire plume and for validation of fire fluid-dynamics codes. However, it is

the joint statistics of temperature and soot that are most useful for assessment of the soot radiative temperature and the radiative emission term in Eq. 1. With this in mind, the single-laser-shot LII soot-volume-fraction data were averaged in a region of pixels coincident with the CARS beam-crossing region, which was located by observing the elastic Rayleigh scattering from the CARS pump beams, as described in Section 3, and verified by generation of a nonresonant CARS signal in a glass cover slip. Using this procedure, we estimated the joint statistics between average soot volume fraction and the enthalpy-pooled temperature in a $\sim 10^{-4}$ cm^3 volume, with a major axis of 10 mm in length. This degree of spatial resolution is superior to previous measurements of joint T/f_v statistics [9, 14, 15], but admittedly falls short of the ideal major-axis length required for full spatial resolution of soot layers of the size shown in Figure 10. For conditions where a soot sheet falls parallel to the axis of the CARS measurement volume, this spatial sampling error is minimized, as in the lower two images of Figure 10, while the effect is maximized when thin soot layers fall mostly normal to the CARS axis.

Mean soot volume fraction conditioned on temperature is estimated by averaging the LII data within 100-K wide temperature bins. Conditional soot f_v results at vertical locations of y = 1.0 and 0.5 m are shown in Figures 14 and 15, respectively. The data at y = 1.5 m are similar to the results at y = 1.0 m and are not shown here. Mean soot data are presented on the left-hand side of the Figures, while the number of realizations within each temperature bin are shown on the right-hand side as a reference to assess the quality of the mean soot results, which are reported for all temperature bins centered from T = 200–2500 K, regardless of the number of samples obtained in each bin. At the extremes of the local temperature pdf, very few samples are obtained and the uncertainty in the mean soot data is significantly elevated. Zero soot is reported if no samples in a temperature bin are recovered. Smooth curves are fit with a five-point running average through the $\langle f_v \mid T \rangle$ data points as a guide, and results are provided at radial positions from plume centerline to r = 40 cm. Over this range of radial locations, the CARS

temperature pdf data in Figure 12 exhibit significant changes, from high-temperature Gaussian-like distributions in the fire interior, uniform distributions in peak mixing zones, to a log-normal temperature distribution with very little high-temperature content at $r \geq 40$ cm. Despite these significant changes in thermal environment, the form of the soot conditional average at $y = 1.0$ m changes very little in the radial direction, which is consistent with recent observations from a turbulent jet flame by Mahmoud *et al.* [6] that soot temperature does not depend substantively upon horizontal position. Mean soot is near zero levels at temperatures below ~1000 K and rises to its peak level at a temperature of 1600-1700 K, with the great majority of soot confined to the range $T = 1000–2000$ K, despite the wide range of temperatures observed over the radial extent of the fire plume. A limited range of soot temperatures is consistent with the behavior observed for a variety of high- and low-sooting fuels in the underfire region of buoyant laboratory-scale flames by Sivathanu and Faeth [9], but the range of soot temperatures observed in Figure 12 is about twice as wide as in their study. The measured soot condtional means in Figure 14 are also remarkably consistent to recent data obtained by Richardson *et al.* [37], who report CARS/LII data from a turbulent C_2H_4 jet flame with a submillimeter-length CARS volume, where soot LII conditioned on temperature peaked at $T = 1700$ K, with little soot observed below $T = 1000$ K.

Lower in the fire plume at $y = 0.5$ m, the form of the conditional soot field again displays the same limited range of soot temperatures from $T = 1000–2000$ K at outward radial positions of $r = 30$ and 40 cm, where CARS measurements indicate a wide range of gas temperatures from $T = 300–2000$ K. However, a wider range of soot temperatures, with measureable low-temperature soot, appears to be present within the vapor-dome region in the fire's interior. At $r = 0$, there is little low-temperature soot simply because very little low-temperature gas penetrates to the center of the fire plume. At $r = 10$ and 15 cm, measureable soot persists into the conditional mean at $T = 600$-900 K with ~100–500 samples in each temperature bin. The conditional mean profiles are essentially uniform for $T = 600$-1400 K, and the

maximum near T = 1600–1700 K is much less pronounced than in the results higher in the plume at y = 1.0 m. Conditional mean soot data at r = 20 cm additionally display a wide range of soot temperatures from T = 400–2000 K, but with a large degree of scatter in the results arising from a reduced number of samples at this location. In general, the distribution of the mean soot temperature appears to transition from a more uniform profile within the interior of the vapor dome region to distribution that is more peaked at T = 1600–1700 K, with little soot below T = 1000 K at more outward radial locations. Our observation of an increased of range of soot temperatures within the vapor-dome region of the fire plume is tempered to some extent by the degree of scatter in the data; nevertheless, a meaningful number (100s) of low-temperature samples was obtained in many cases with measurable soot persisting into the conditional mean at r = 10–20 cm. Observation of a wide range of soot temperatures low in the fire plume contrasts reported laboratory-scale observations. Turbulent jet-flame measurements by Mahmoud *et al.* [6] and buoyant flame data reported by Sivathanu and Faeth [9] both show that soot exists in a relatively narrow range of high temperatures close to its inception point low in the flame and then evolves to experience a significant increase in low-temperature content as it convects vertically. The opposite trend is observed in this pool fire, which raises several questions. Soot is likely not formed low in the fire plume at such low (T < 1000 K) temperatures. Any mechanism for transport of cold soot into the fire interior within the vapor dome at y = 0.5 m is unclear, as is the reason why a broader range of soot temperatures does not persist with transport to higher positions within the more actively burning region of the fire at y = 1.0 and 1.5 m.

We additionally estimate the form of the joint temperature-soot pdf. Two estimates are performed, with the results shown in Figure 16. The largest sample of data is obtained from the actively burning region of the fire plume at y = 1.0 and 1.5 m and r = 0–40 cm, where the soot conditional mean displays the behavior seen in Figure 14. This result is shown in the upper plot of Figure 16. A second pdf

estimate based on a smaller sample of data within the vapor-dome region at y = 0.5 m and r = 0–20 cm, where a wider range of soot temperatures is observed in the conditional mean results, is shown in the lower portion of Figure 16. Data from multiple spatial locations were combined to maximize statistical convergence. Despite the large number of several hundred thousand single-laser-shot measurements acquired over the course of the measurement campaign, sampling errors for conditional soot statistics are still significant because the high degree of intermittency in the soot fluctuations results in a large number of realizations with zero soot. This procedure is somewhat validated by the consistency of the structure of the soot conditional mean data of Figures 14 and 15 across a wide range of spatial locations. Naturally, the joint pdf is consistent with the pdf of the total soot f_v fluctuations in Figure 13 and the temperature-conditioned mean soot data of Figures 14 and 15. Across all temperatures, the soot pdf displays a zero-clipped structure. Soot is most concentrated in the temperature bands T = 1500–1800 K and T = 1200–1500 K. The least populated soot temperature bins are in the T = 300–900 K and 2100–2400 K ranges, which would be expected based on the concentration of the soot conditional mean data in the T = 1000–2000 K range. Some increase in the likelihood of low-temperature, T = 300–900 K, is observed for the joint pdf in the vapor-dome region.

5. Summary and Conclusion

We have presented the results of a recent data campaign in which high-fidelity laser diagnostics have been used to obtain spatial maps of temperature and soot statistics in a buoyant, liquid-fueled pool fire of meaningful meter-scale size. The experiments were performed in a 2-m base diameter fire plume with a 10%-toluene/90%-methanol fuel blend that was selected as a reasonable compromise between fuel sooting propensity and facilitation of laser-diagnostic measurements. The resulting fire plume was of

sufficient size to provide turbulence properties relevant to large-scale accident scenarios, but at a reduced soot loading relative to real transportation fuels.

Dual-pump CARS and LII were used to obtain single-laser-shot thermodynamic mean temperatures and soot-volume-fraction data with volumetric spatial resolutions of 10^{-4} and 10^{-5} cm^3, respectively. Rayleigh scattering thermometry in a pure methanol fire with similar turbulence properties revealed modest thermal gradients within the 8–10 mm long CARS measurement volume, so that CARS temperatures closely approximated thermodynamic-mean values. Extensive ensembles of single-laser-shot data acquired over many different pool-fire experiments allowed us to construct radial profiles of mean and rms fluctuating quantities and probability densities at heights of 0.5, 1.0 and 1.5 m above the liquid fuel surface. Evolution of the temperature pdf structures reveals a gradual transition from a hot-gas region at the center of the fire plume, with limited mixing with outside air and near-Gaussian pdf structure, to an intermediate region with uniform pdf, and finally to a highly intermittent region with lognormal pdf. Soot pdf structure is zero-clipped at all locations throughout the plume, indicative of a high degree of intermittency in the soot fluctuations and consistent with LII measurements performed in smaller laboratory scale buoyant flame systems and jet flames [4, 5, 7, 12, 13, 38], but in contrast to heavily sooting meter-scale fire experiments performed with real JP-8 transportation fuel [14, 15], which indicate low soot intermittency in the interior of the fire, that transitions to a more intermittent character at the fire boundaries.

Estimates of the joint statistics between the CARS temperature and the average soot volume fraction within the CARS measurement volume reveal that soot is present in a limited temperature range of T = 1000–2000 K at all radial locations within the actively burning region of the pool fire at y = 1.0 and 1.5 m above the liquid fuel surface. Lower in the fire plume, at y = 0.5 m, soot appears encompass a wider range of temperatures from $T \sim$ 400–2000 K within the interior of the fire for $r \leq 20$ cm,

corresponding to the hydrocarbon-rich vapor-dome region. This contrasts with measurements in laboratory turbulent flames [6, 9], which show that soot occupies a narrow range of temperatures near inception low in the flame and progress to a wider range of thermal environments with upward transport. The joint pdf of the temperature and soot fluctuations was estimated by combining data over multiple spatial locations, revealing that soot temperatures of T = 1500 to 1800 K are most likely at all measurement stations throughout the pool fire.

Acknowledgements

The authors are grateful to the late Sheldon R. Tieszen of Sandia for his mentorship, many stimulating conversations regarding the physics of fire plumes, and for his stalwart support of this project. The support of the operations staff at the Sandia FLAME facility, Dann Jernigan, Ciro Ramirez, and Martin Sanchez is gratefully acknowledged. We also thank Kraig Frederickson, currently at the Ohio State University, for his work on diagnostic development during his time at Sandia. This work is supported by Sandia National Laboratories and the United States Department of Energy. Sandia National Laboratories is a multi-program laboratory managed and operated by Sandia Corporation, a wholly owned subsidiary of Lockheed-Martin Company, for the U.S. Department of Energy's National Nuclear Security Administration under contract DE-AC04-94AL85000.

References

1. V. I. Blinov; G. N. Khyudiakov, U.S. Army Engineering Research and Development Laboratories, Report AERDL-T-1490-A, Fort Belvoir, VA, 1961.
2. H. C. Hottel, Fire Research Abstracts and Reviews 1 (1959) 41-44.
3. M. F. Modest, Radiative Heat Transfer, McGraw-Hill, 1993.
4. Y. Xin; J. P. Gore, Proceedings of the Combustion Institute 30 (2005) 719-726.
5. N. H. Qamar; Z. T. Alwahabi; Q. N. Chan; G. J. Nathan; D. Roekaerts; K. D. King, Combustion and Flame 156 (2009) 1339-1347.
6. S. M. Mahmoud; G. J. Nathan; P. R. Medwell; B. B. Dally; Z. T. Alwahabi, Proceedings of the Combustion Institute 35 (2015) 1931-1938.
7. T. L. Henriksen; G. J. Nathan; Z. T. Alwahabi; N. Qamar; T. A. Ring; E. G. Eddings, Combustion and Flame 156 (2009) 1480-1492.
8. K. Frederickson; S. P. Kearney; T. W. Grasser, Applied Optics 50 (2011) A49-A59.
9. Y. R. Sivathanu; G. M. Faeth, Combustion and Flame 81 (1990) 150-165.
10. Y. R. Sivathanu; J. P. Gore; G. M. Faeth, Combustion and Flame (73) (1988) 315-329.
11. Y. R. Sivathanu; G. M. Faeth, Combustion and Flame 81 (1990) 133-149.
12. M. Köhler; K. P. Geigle; W. Meier; B. M. Crosland; K. A. Thomson; G. J. Smallwood, Applied Physics B 104 (2011) 409-425.
13. C. R. Shaddix; J. Zhang; R. W. Schefer; J. Doom; J. C. Oefelein; S. Kook; L. M. Pickett; H. Wang, SAND2010-7178, Sandia National Laboratories, Livermore, CA, 2010.
14. L. A. Gritzo; Y. R. Sivathanu; W. Gill, Combustion Science and Technology 139 (1998) 113-136.
15. J. J. Murphy; C. R. Shaddix, Combustion Science and Technology 178 (2006) 865-894.
16. S. P. Kearney; K. Frederickson; T. W. Grasser, Proceedings of the Combustion Institute 32 (2009) 871-878.
17. K. Frederickson; S. P. Kearney; A. Luketa; J. C. Hewson; T. W. Grasser, Combustion Science and Technology 182 (2010) 941-959.
18. K. Frederickson; S. P. Kearney; T. W. Grasser, Applied Optics 50 (4) (2011) A49-A59.
19. T. K. Blanchat; T. J. O'Hern; S. P. Kearney; A. Ricks; D. Jernigan, Proceedings of the Combustion Institute 32 (2) (2009) 2511-2518.
20. S. R. Tieszen; T. J. O'Hern; E. J. Weckman; R. W. Schefer, Combustion and Flame 139 (2004) 126-141.
21. A. C. Eckbreth, Applied Physics Letters 32 (1978) 421-423.
22. P. E. Bengtsson; M. Alden, Combustion and Flame 80 (1990) 322-328.
23. S. P. Kearney; M. N. Jackson, AIAA Journal 45 (12) (2007) 2947-2956.
24. R. E. Palmer, SAND89-8206, Sandia National Laboratories: Livermore, CA, 1989.
25. J. Bonamy; L. Bonamy; D. Robert; M. L. Gonze; G. Millot; B. Lavorel; H. Berger, Journal of Chemical Physics 94 (1991) 6584-6589 10.1063/1.460285.
26. R. D. Hancock; K. E. Bertagnolli; R. P. Lucht, Combustion and Flame 109 (1997) 323-331.
27. J. Y. Zhu; D. Dunn-Rankin, Applied Physics B 56 (1993) 47-55.
28. J. P. Boquillon; M. Péalat; P. Bouchardy; G. Collin; P. Magre; J. P. Taran, Optics Letters 13 (9) (1988) 722-724.
29. P. Magre; P. Moreau; G. Collin; R. Borghi; M. Péalat, Combustion and Flame 71 (1988) 147-168.

30. R. J. Santoro; C. R. Shaddix, in: Applied Combustion Diagnostics, K. K. Hoinghaus; J. B. Jeffries, (Eds.) Taylor and Francis: 2002; pp 252-286.
31. T. Ni; J. A. Pinson; S. Gupta; R. J. Santoro, Applied Optics 34 (30) (1995) 7083-7091.
32. R. J. Santoro; H. G. Semerjian; R. A. Dobbins, Combustion and Flame 51 (1983) 203-218.
33. E. Nordström; N. E. Olofsson; J. Simonsson; J. Johnsson; H. Bladh; P. E. Bengtsson, Proceedings of the Combustion Institute 35 (2015) 3707-3713.
34. L. A. Gritzo; W. Gill; V. F. Nicolette, SAND97-Sandia National Laboratories: Albuqueque, NM and Livermore, CA, 1997.
35. T. Blanchat; D. Jernigan, SAND2016-0224, Sandia National Laboratories: Albuquerque, NM, 2016.
36. T. J. O'Hern; E. J. Weckman; A. L. Gerhart; S. R. Tieszen; R. W. Schefer, Journal of Fluid Mechanics 544 (2005) 143-171
37. D. R. Richardson; S. Roy; J. R. Gord, to be published (2017)
38. S. Y. Lee; S. R. Turns; R. J. Santoro, Combustion and Flame 156 (2009) 2264-2275

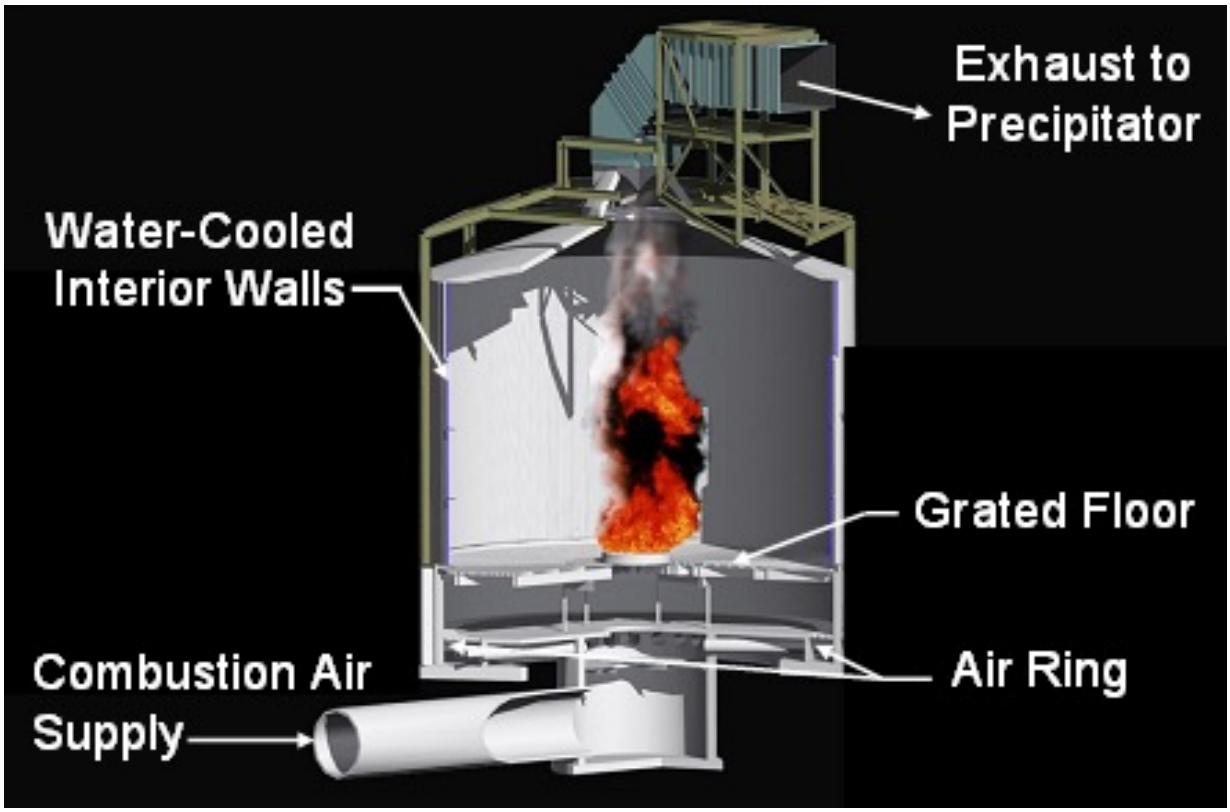

Figure 1 – Essential elements of the FLAME test bay.

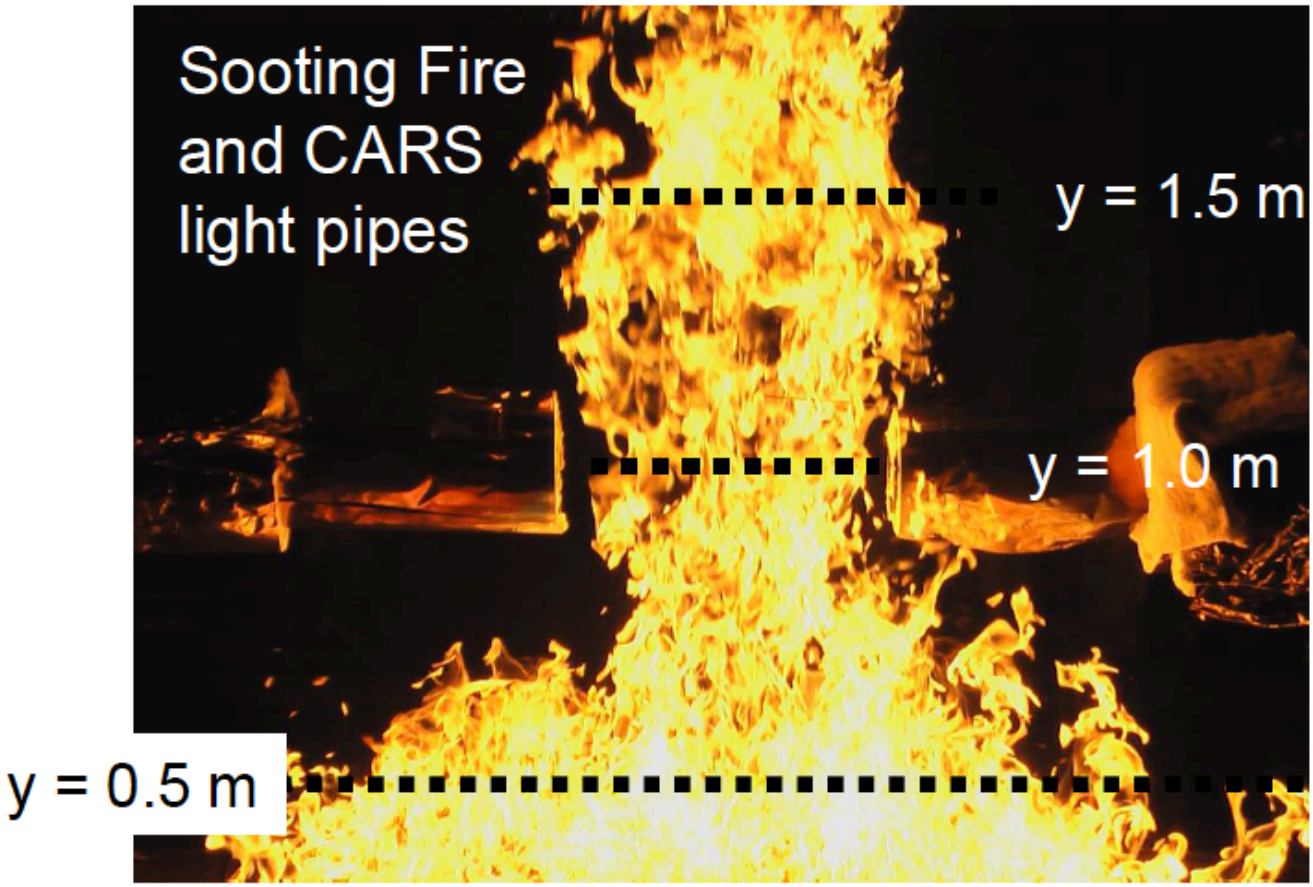

Figure 2 – Digital photograph of the 2-m diameter, 10% toluene/90% methanol pool fire. The large-diameter light pipes are representative of an early experiment and were significantly reduced for the measurement campaign discussed here.

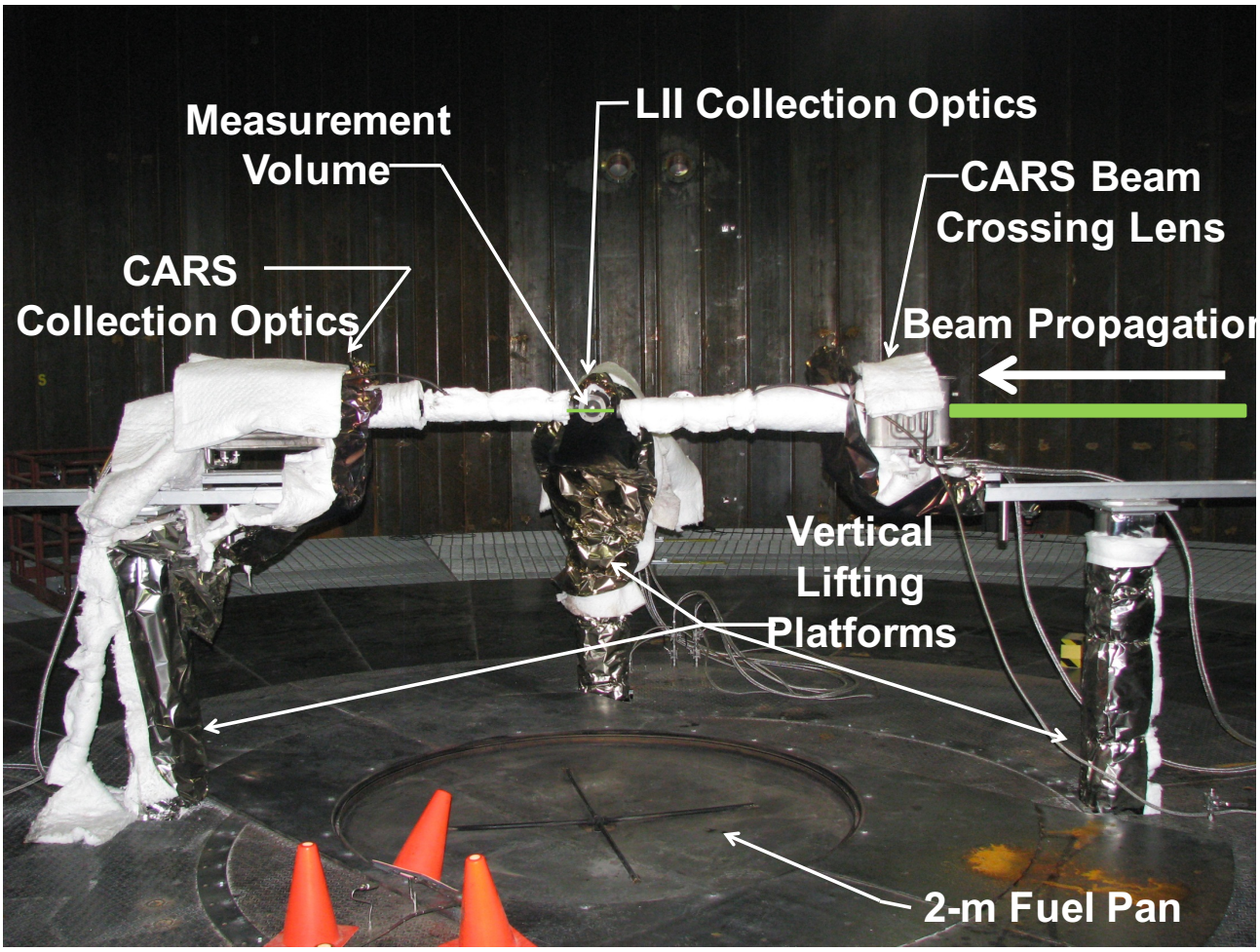

Figure 3 –Digital photograph of the FLAME test bay as configured for the measurements reported here.

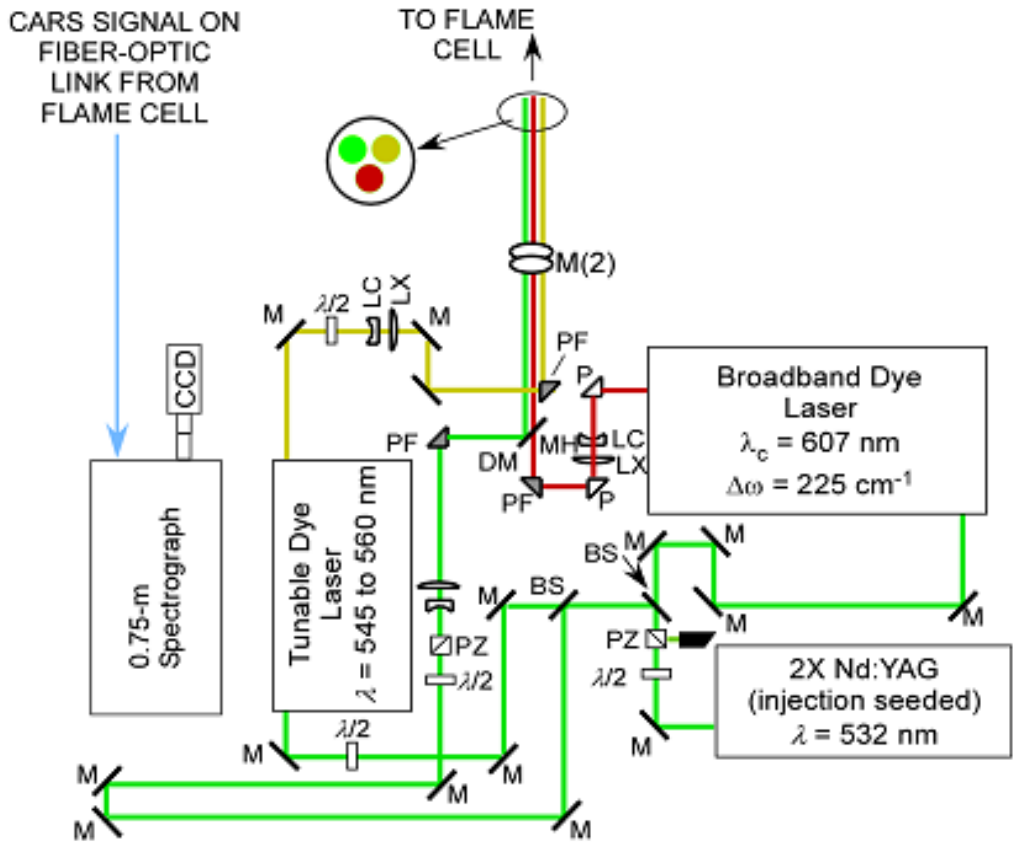

Figure 4 – Dual-pump CARS instrument as fielded at the Sandia FLAME facility. The arrangement of the laser and optical system in the west laboratory is shown. Legend is as follows: (BS) beam-splitter; (M) dielectric turning mirror; (M2) mirror periscope; (LC) concave lens; (LX) convex lens; (P) turning prism; (PF) turning prism on fine-adjust mount; (PZ) polarizer; (λ/2) half-wave rotator.

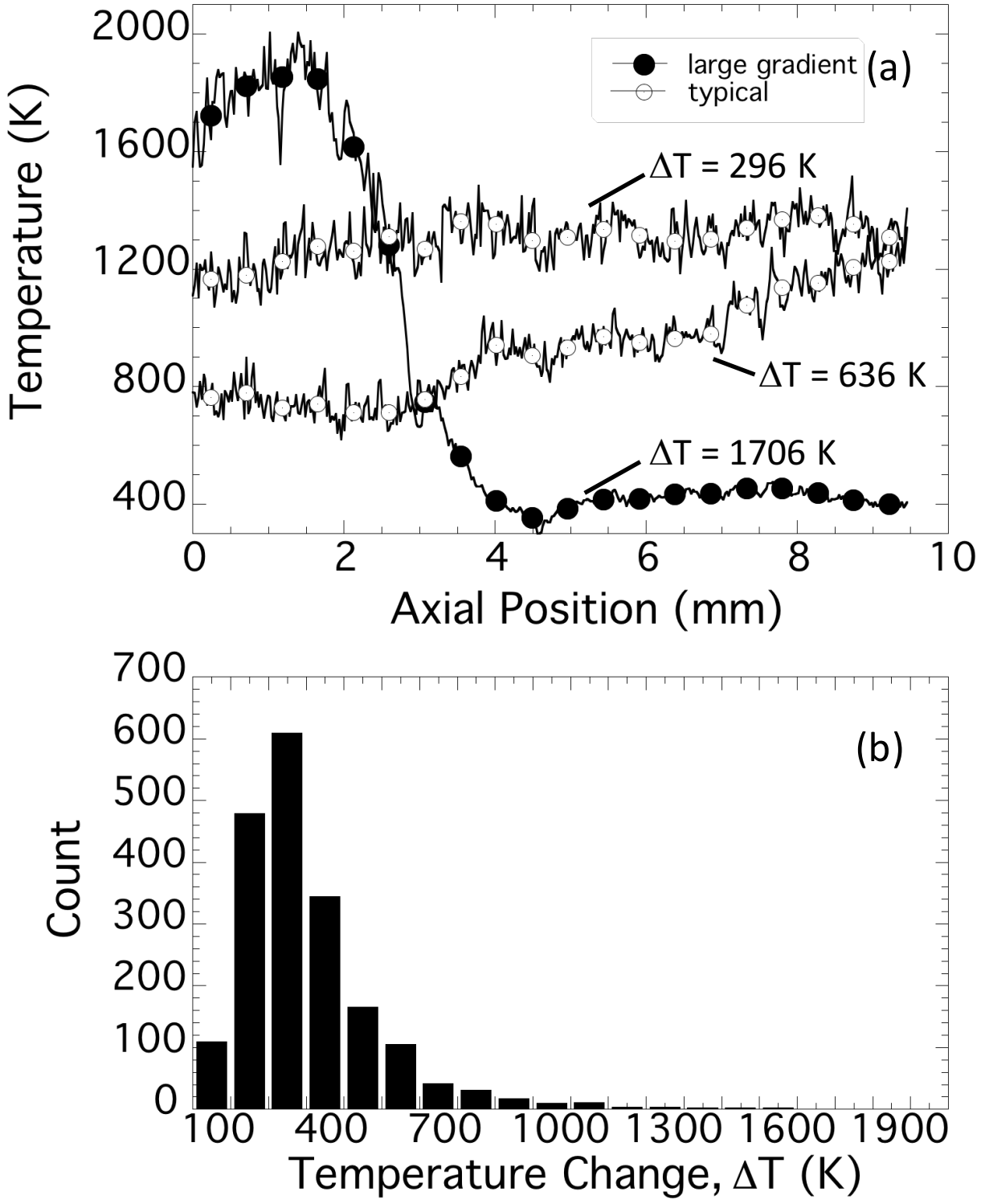

Figure 5 – Sample Rayleigh-measured temperature profiles along the axis of the CARS measurement volume at the radial center of a methanol pool fire (a). Histogram of the temperature change, ΔT, along the CARS volume axis.

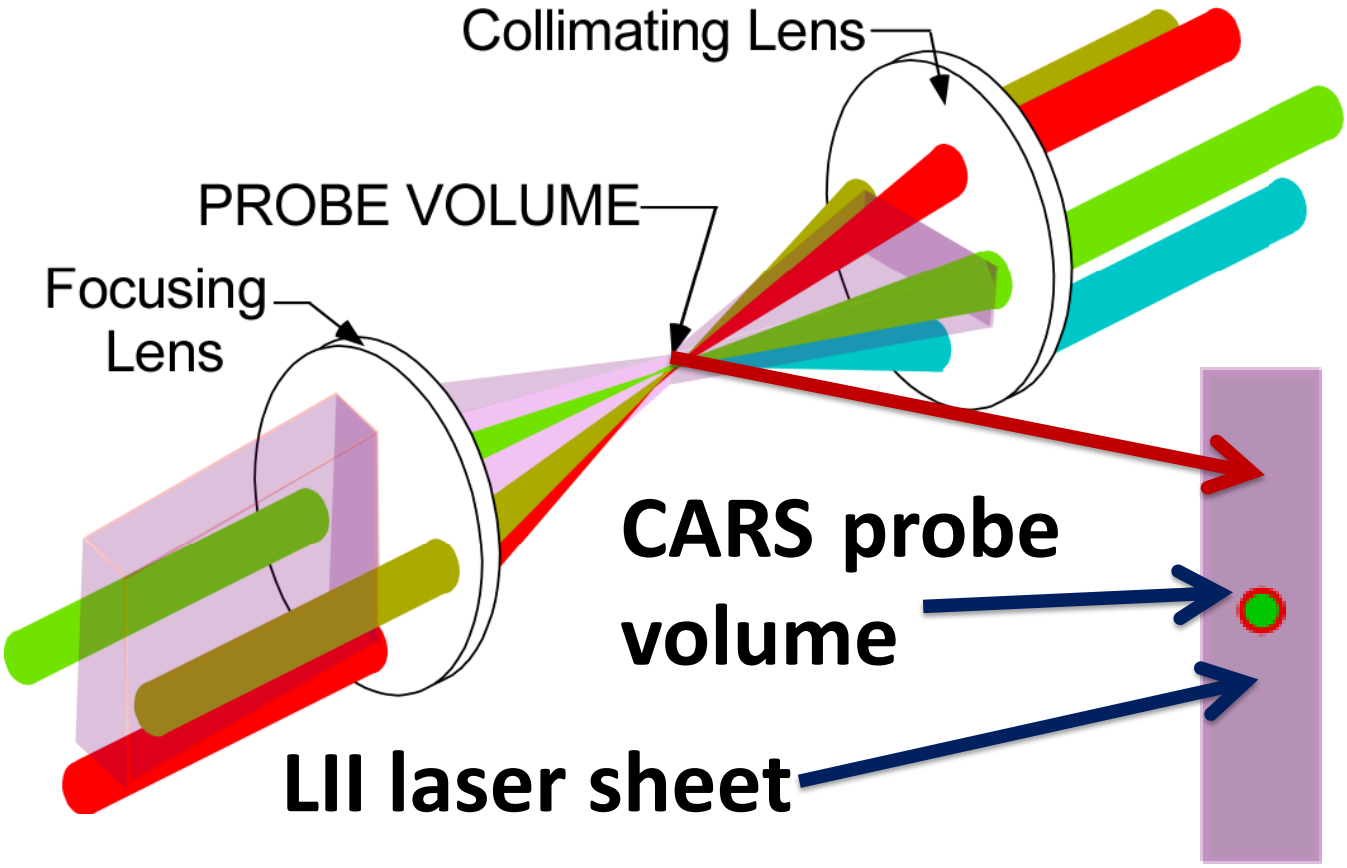

Figure 6 – Arrangement of CARS laser beams and the coincident LII laser sheet.

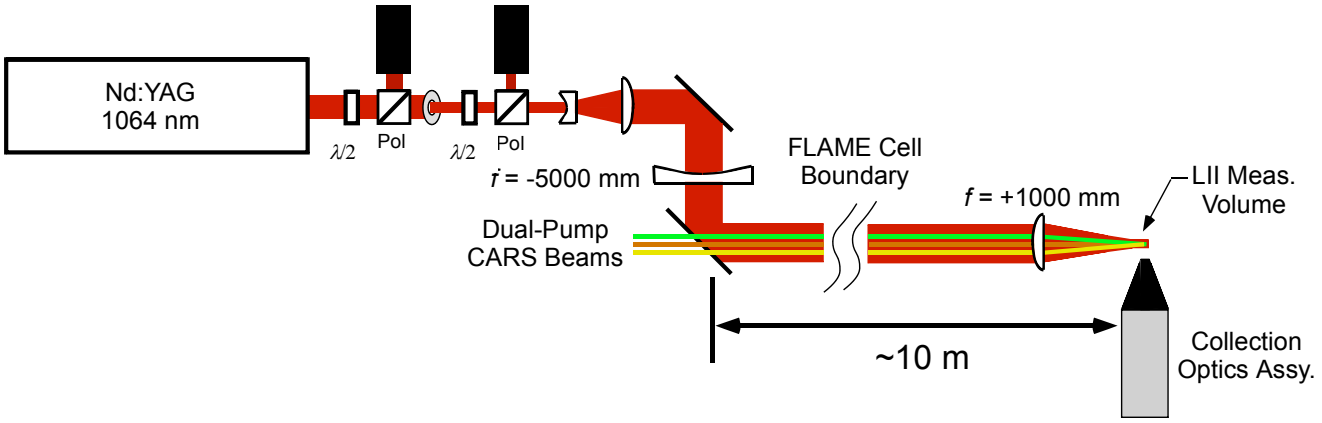

Figure 7 – Schematic of the LII laser-sheet delivery optics at FLAME.

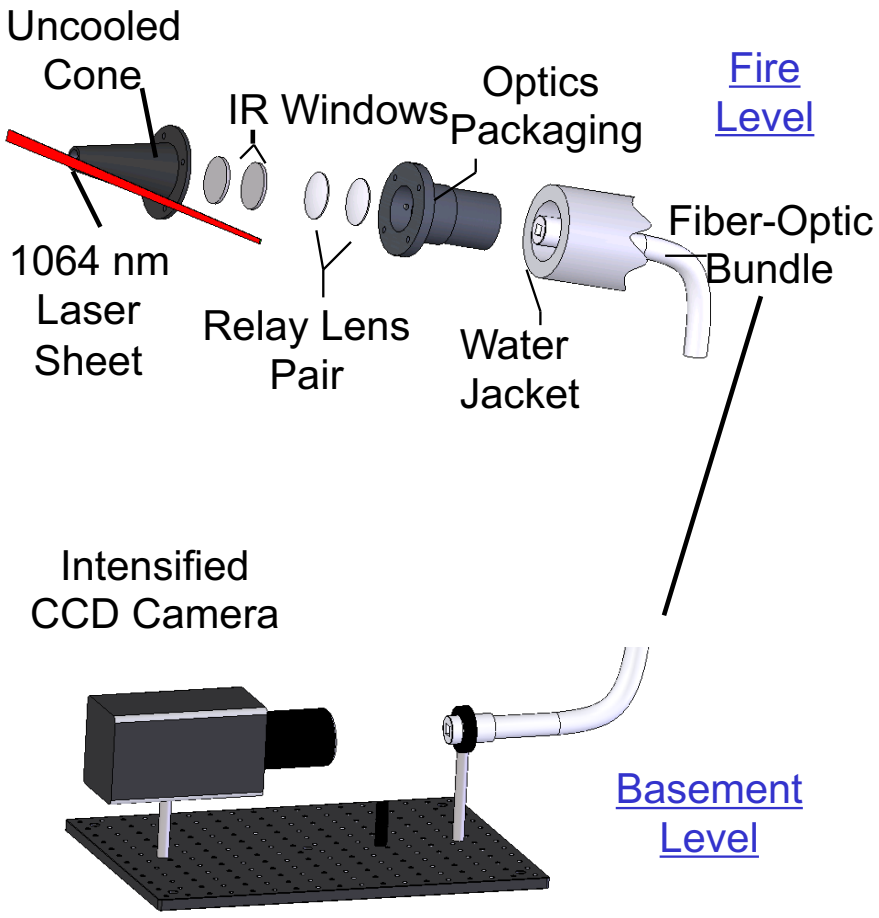

Figure 8 – Collection optics for LII at FLAME.

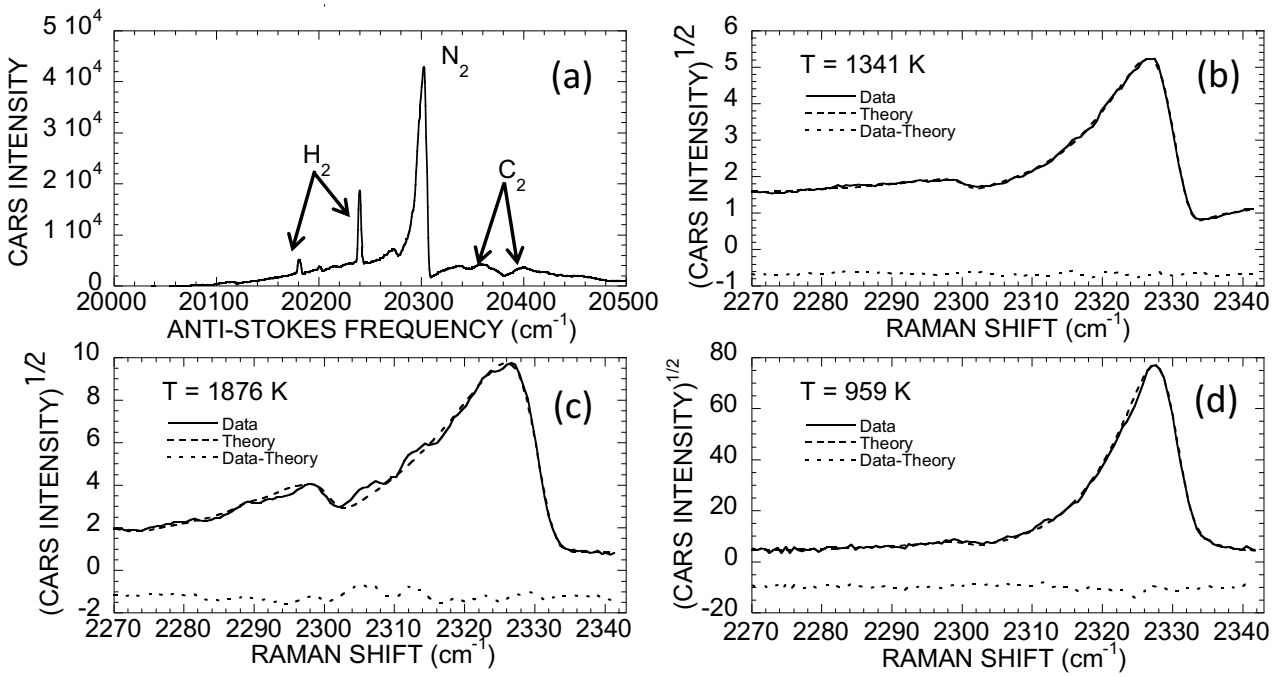

Figure 9 – Shot-averaged CARS spectrum from the center of the fire plume within the fuel-rich "vapor dome" region at y = 0.5 m (a). Single-laser-shot N_2 CARS spectra from the vapor dome region (b,c) and single-shot spectrum at y = 0.5 m above the fuel surface and x = 60 cm from the center of the fire plume.

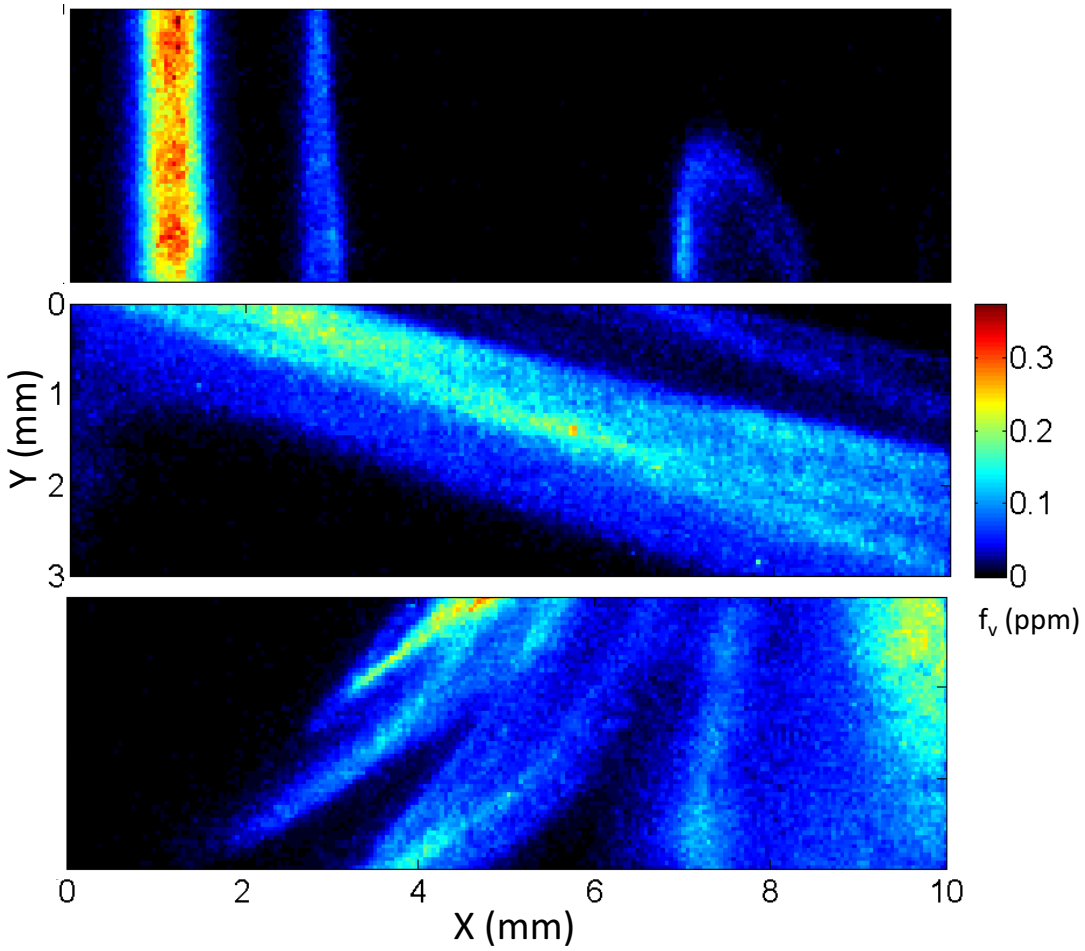

Figure 10 – Representative single-laser-shot soot LII images.

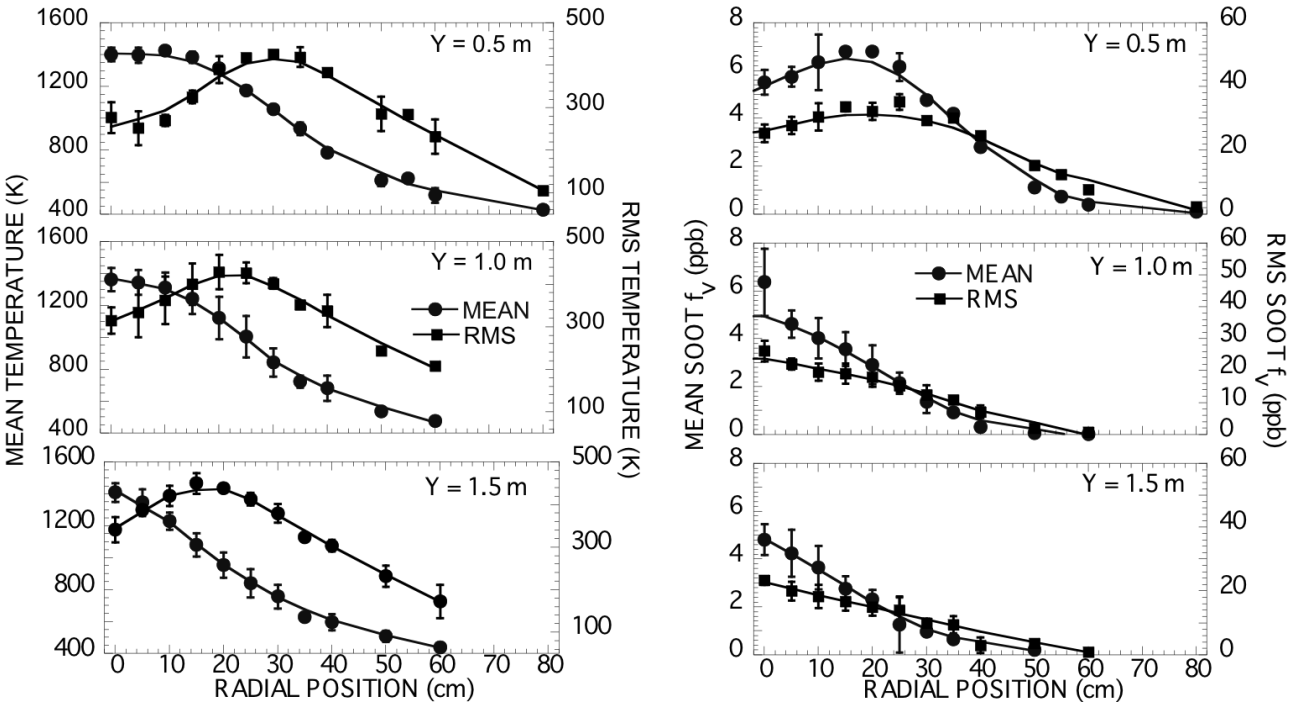

Figure 11 – Radial distributions of the time-mean and route-mean-square fluctuations of the temperature (left) and soot-volume-fraction (right) in a 2-m-diameter toluene/methanol pool fire. Data are presented at three different heights above the liquid fuel surface as indicated by the values of *Y* on the plots.

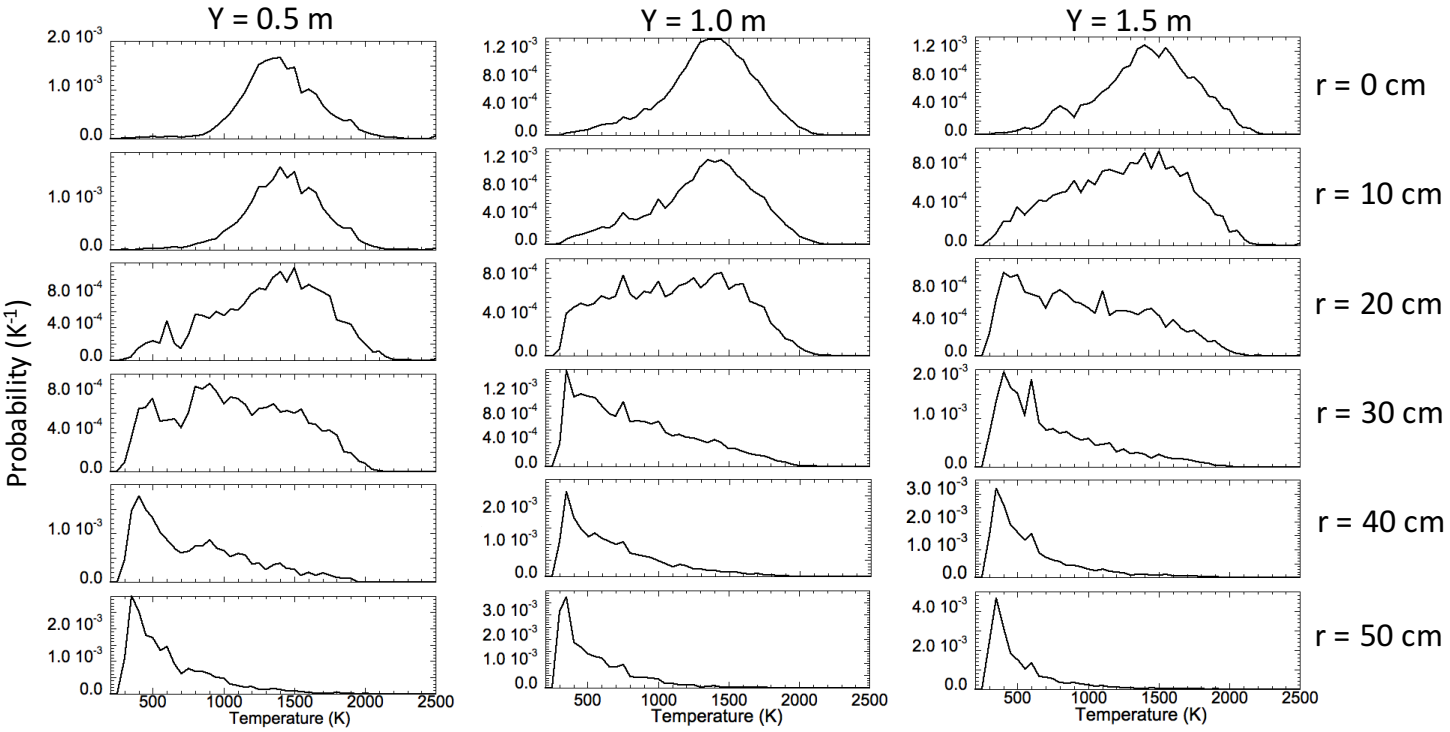

Figure 12 – Probability density functions (pdf) of the temperature fluctuations in a 2-m-diameter methanol/toluene pool fire. Each column represents the radial distribution of the pdf for the height above the liquid fuel surface, *Y*, indicated at the top.

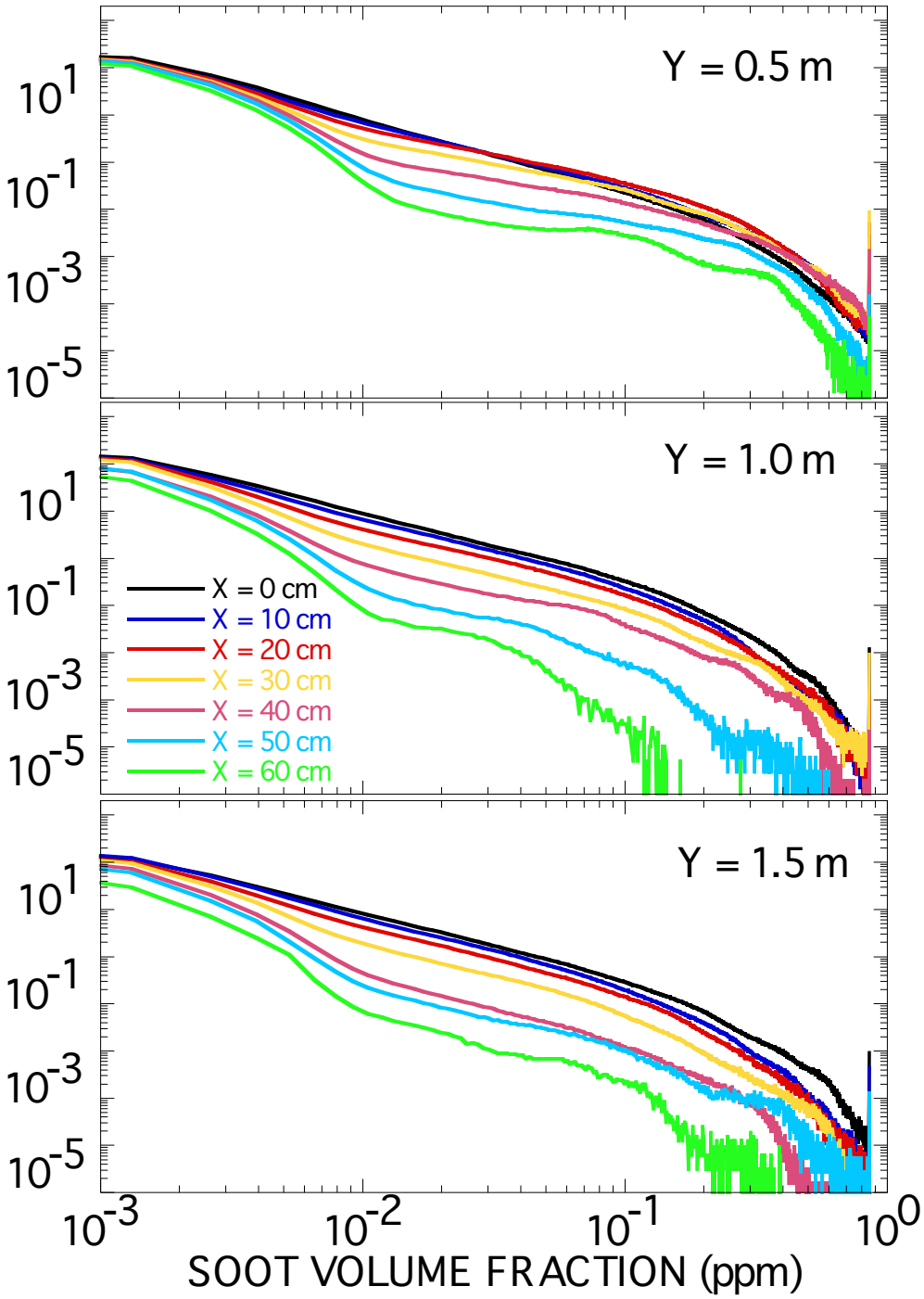

Figure 13 – Probability density function (pdf) of the soot-volume-fraction fluctuations in a 2-m-diameter methanol/toluene pool fire. Each plot displays the radial evolution of the soot pdf at the height above the liquid fuel level, *Y*, indicated on the plots.

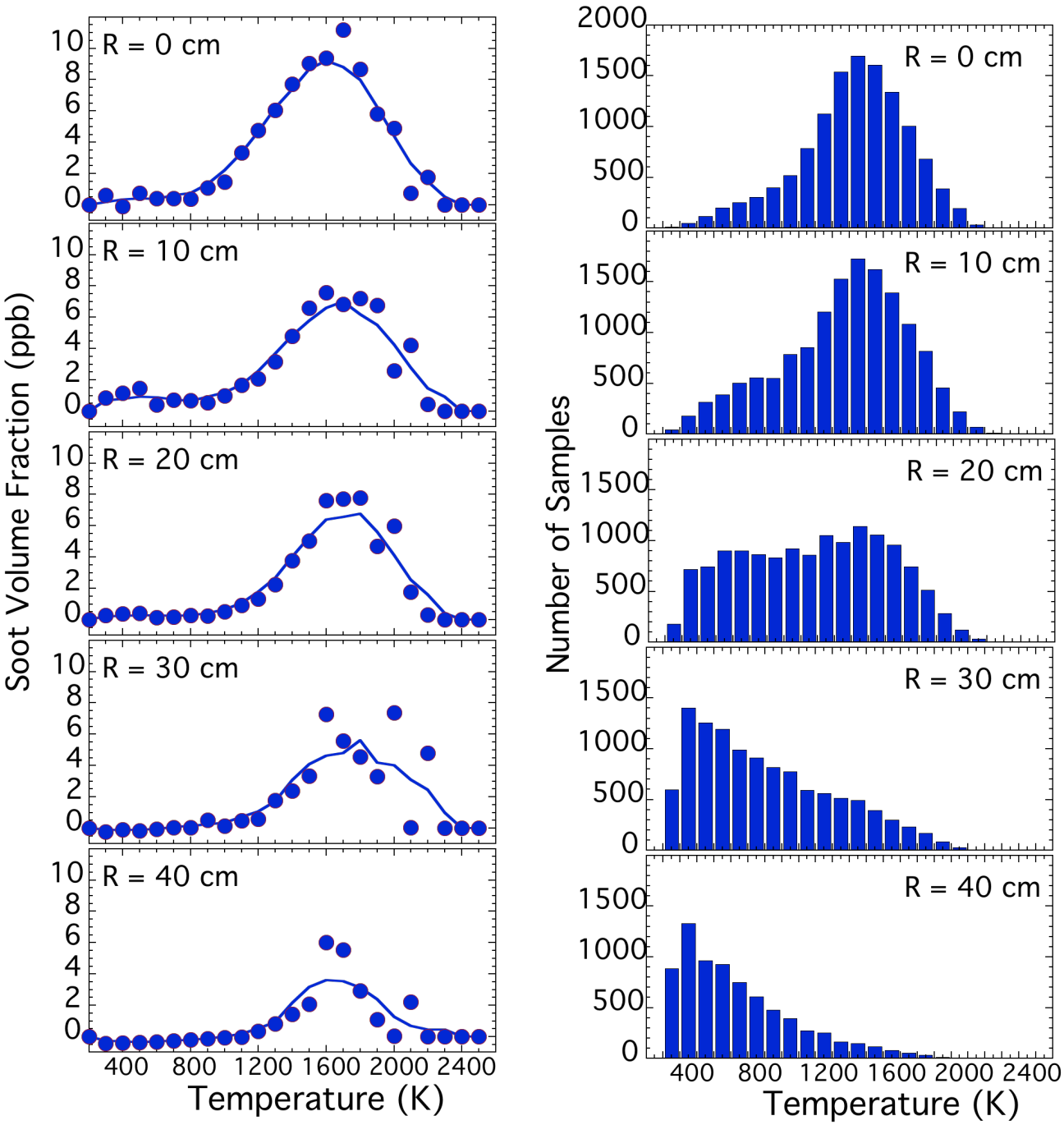

Figure 14 – Mean soot-volume-fractions conditioned on CARS temperature at a height of y = 1.0 m above the liquid fuel surface.

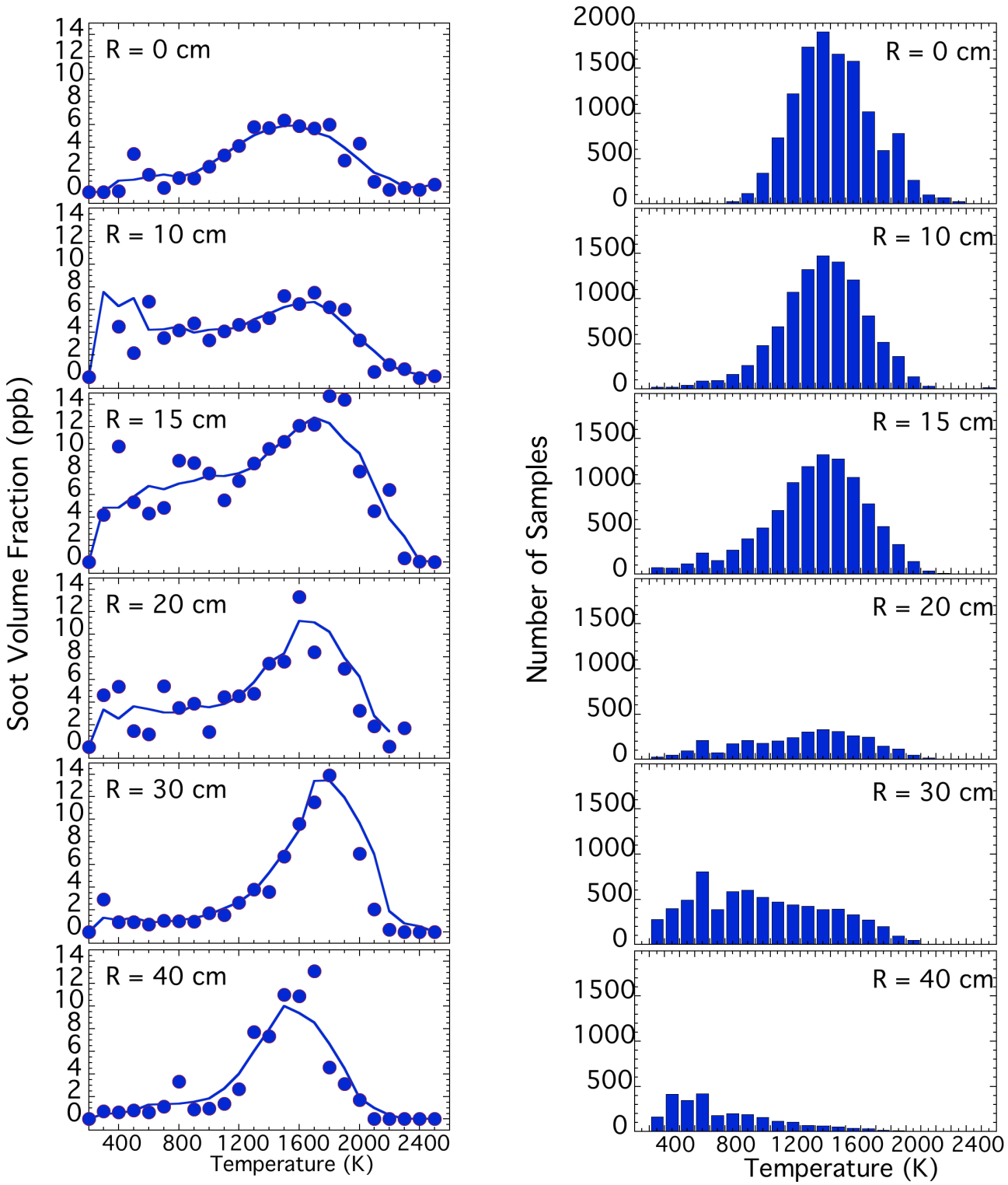

Figure 15 – Mean soot-volume-fractions conditioned on CARS temperature at a height of y = 0.5 m above the liquid fuel surface.

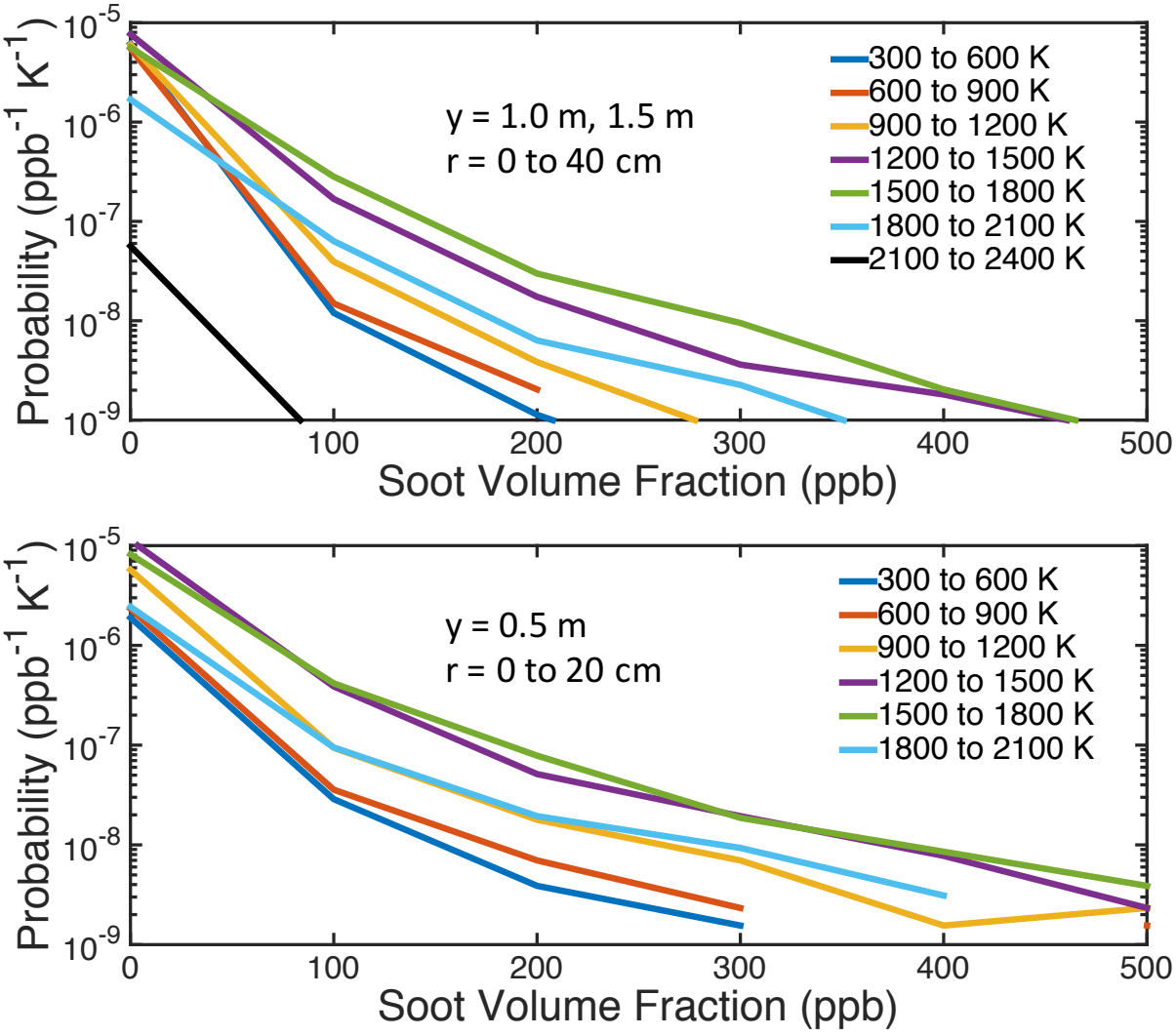

Figure 16 – Estimate of the joint temperature/soot pdf obtained by pooling joint CARS/LII measurements from multiple spatial locations. The upper plot shows results from the actively burning region at y = 1.0 and 1.5 m. The lower plot shows results from the vapor-dome region.